

# Abundance analysis, spectral variability, and search for the presence of a magnetic field in the typical PGa star HD 19400

S. Hubrig,<sup>1★</sup> F. Castelli,<sup>2</sup> J. F. González,<sup>3</sup> T. A. Carroll,<sup>1</sup> I. Ilyin,<sup>1</sup> M. Schöller,<sup>4</sup>  
N. A. Drake,<sup>5,6</sup> H. Korhonen<sup>7</sup> and M. Briquet<sup>8</sup>

<sup>1</sup>Leibniz-Institut für Astrophysik Potsdam (AIP), An der Sternwarte 16, D-14482 Potsdam, Germany

<sup>2</sup>Istituto Nazionale di Astrofisica, Osservatorio Astronomico di Trieste, via Tiepolo 11, I-34143 Trieste, Italy

<sup>3</sup>Instituto de Ciencias Astronómicas, de la Tierra, y del Espacio (ICATE), 5400 San Juan, Argentina

<sup>4</sup>European Southern Observatory, Karl-Schwarzschild-Str. 2, D-85748 Garching bei München, Germany

<sup>5</sup>Sobolev Astronomical Institute, St Petersburg State University, Universitetski pr. 28, 198504 St Petersburg, Russia

<sup>6</sup>Observatório Nacional/MCTI, Rua José Cristino 77, CEP 20921-400 São Cristóvão, Rio de Janeiro, RJ, Brazil

<sup>7</sup>Finnish Centre for Astronomy with ESO (FINCA), University of Turku, Väisälöntie 20, FI-21500 Piikkiö, Finland

<sup>8</sup>Institut d'Astrophysique et de Géophysique, Université de Liège, Allée du 6 Août 17, Sart-Tilman, Bât. B5C, B-4000 Liège, Belgium

Accepted 2014 June 4. Received 2014 June 4; in original form 2014 March 1

## ABSTRACT

The aim of this study is to carry out an abundance determination, to search for spectral variability and for the presence of a weak magnetic field in the typical PGa star HD 19400. High-resolution, high signal-to-noise High Accuracy Radial-velocity Planet Searcher (HARPS) spectropolarimetric observations of HD 19400 were obtained at three different epochs in 2011 and 2013. For the first time, we present abundances of various elements determined using an ATLAS12 model, including the abundances of a number of elements not analysed by previous studies, such as Ne I, Ga II, and Xe II. Several lines of As II are also present in the spectra of HD 19400. To study the variability, we compared the behaviour of the line profiles of various elements. We report on the first detection of anomalous shapes of line profiles belonging to Mn and Hg, and the variability of the line profiles belonging to the elements Hg, P, Mn, Fe, and Ga. We suggest that the variability of the line profiles of these elements is caused by their non-uniform surface distribution, similar to the presence of chemical spots detected in HgMn stars. The search for the presence of a magnetic field was carried out using the moment technique and the Singular Value Decomposition (SVD) method. Our measurements of the magnetic field with the moment technique using 22 Mn II lines indicate the potential existence of a weak variable longitudinal magnetic field on the first epoch. The SVD method applied to the Mn II lines indicates  $\langle B_z \rangle = -76 \pm 25$  G on the first epoch, and at the same epoch the SVD analysis of the observations using the Fe II lines shows  $\langle B_z \rangle = -91 \pm 35$  G. The calculated false alarm probability values, 0.008 and 0.003, respectively, are above the value  $10^{-3}$ , indicating no detection.

**Key words:** stars: abundances – stars: atmospheres – stars: chemically peculiar – stars: individual: HD 19400 – stars: magnetic field – stars: variables: general.

## 1 INTRODUCTION

A number of chemically peculiar stars with spectral types B7–B9 exhibit in their atmospheres large excesses of P, Mn, Ga, Br, Sr, Y, Zr, Rh, Pd, Xe, Pr, Yb, W, Re, Os, Pt, Au, and Hg, and underabundances of He, Al, Zn, Ni, and Co (e.g. Castelli & Hubrig 2004). These stars are usually called the HgMn stars. The aspect of inhomogeneous distribution of some chemical elements over the surface

of HgMn stars was first discussed by Hubrig & Mathys (1995). From a survey of HgMn stars in close spectroscopic binaries, they suggested that some chemical elements might be inhomogeneously distributed on the surface, with, in particular, preferential concentration of Hg along the equator. Recent studies revealed that not only Hg, but also many other elements, most typically Ti, Cr, Fe, Mn, Sr, Y, and Pt, are concentrated in spots of diverse size, and different elements exhibit different abundance distributions across the stellar surface (e.g. Hubrig et al. 2006b; Briquet et al. 2010; Makaganiuk et al. 2011b; Korhonen et al. 2013). In SB2 systems, the hemispheres of components facing each other usually

★ E-mail: shubrig@aip.de

display low-abundance element spots, or no spots at all (e.g. Hubrig et al. 2010). Moreover, evolution of the abundance spots of several elements at different time-scales was discovered in a few HgMn stars: Briquet et al. (2010) and Korhonen et al. (2013) reported the presence of dynamical spot evolution over a couple of weeks for the SB1 system HD 11753, while Hubrig et al. (2010) detected a secular element evolution in the double-lined eclipsing binary AR Aur.

However, not much is known about the behaviour of different elements in the hotter extension of the HgMn stars, the PGa stars, with rich P II, Mn II, Ga II, and Hg II spectra, and effective temperatures of about 13 500 K and higher (e.g. Alonso et al. 2003; Rachkovskaya, Lyubimkov & Rostopchin 2006).

During our observing run in 2013 July, we obtained a high-resolution, high signal-to-noise (S/N) polarimetric High Accuracy Radial-velocity Planet Searcher (HARPS) spectrum of the typical PGa star HD 19400. We downloaded two additional polarimetric spectra of this star, obtained on two consecutive nights in 2011 December, from the ESO archive. These spectra were used to carry out an abundance analysis and to investigate whether HD 19400, similar to HgMn stars, exhibits a weak magnetic field and an inhomogeneous distribution of various elements over the stellar surface. Notably, Maitzen (1984) suggested the presence of a magnetic field in this star using observations of the  $\lambda 5200$  feature. A careful inspection of the spectra acquired on three different epochs revealed the presence of anomalous flat-bottom line profiles belonging to the overabundant elements Hg and Mn (Drake et al. 2013), reminiscent of profile shapes observed in numerous HgMn stars (e.g. Hubrig et al. 2006b, 2011; Makaganiuk et al. 2011b). Moreover, these observations revealed the variability of line profiles belonging to Hg II, Mn II, P II, Fe II, and Ga II. Dommangen & Nys (2002) mention in the CCDM catalogue a nearby component at a separation of 0.1 arcsec and a position angle of  $179^\circ$ . However, no lines belonging to the secondary were detected in the previous spectral studies, indicating that HD 19400 can be treated as a single star. In the following sections, we discuss the results of the abundance determination, the spectral variability detected in the lines of certain elements and our search for the presence of a weak magnetic field.

## 2 OBSERVATIONS

All three spectropolarimetric observations have been obtained with the HARPS polarimeter (HARPSpol; Snik et al. 2008) attached to ESO's 3.6 m telescope (La Silla, Chile). Two spectropolarimetric observations have been obtained on two consecutive nights on 2011 December 15 and 16, and one on 2013 July 19. The obtained polarimetric observations with a S/N between 500 and 600 in the Stokes  $I$  spectra and a resolving power of about  $R = 115\,000$  cover the spectral range 3780–6910 Å, with a small gap between 5259 and 5337 Å. Each polarimetric observation consists of several subexposures, obtained with different orientations of the quarter-wave retarder plate relative to the beam splitter of the circular polarimeter. The reduction and calibration of archive spectra were performed using the HARPS data reduction software available at the ESO headquarter in Germany, while the spectra obtained in 2013 July have been reduced using the pipeline available at the 3.6 m telescope in Chile.

To normalize the HARPS spectra to the continuum level, we used the image of the extracted echelle orders. First, we fit a continuum spline in columns of the image in cross-dispersion direction. Each column is fitted in a number of subsequent iterations until it converges to the same upper envelope of the continuum level. After each iteration, we analyse the residuals of the fit and make a robust estimation of the noise level based upon a statistical test of the

**Table 1.** Logbook of the HARPS polarimetric observations, including the modified Julian date of mid-exposure followed by the achieved signal-to-noise ratio.

MJD	S/N <sub>4500</sub>
55910.054	820
55911.042	760
56492.327	470

symmetric part of the distribution. All pixels whose residuals are below the specified sigma clipping level are masked out from the subsequent fit. This way the smooth spline function is rejecting all spectral lines below, but leaving the continuum pixels to fit. Once all columns are processed, we fit the resulting smoothed curves in the dispersion direction by using the same approach with the robust noise estimation from the residuals, but this time rejecting possible outliers above and below the specified sigma clipping level. As a result, we create a bound surface with continuous first derivatives in the columns and rows. We employ a smoothing spline with adaptive optimal regularisation parameters, which selects the minimum of the curvature integral of the smoothing spline. As a test for the validity of the continuum fit, we check whether the normalized overlapping echelle orders are in good agreement with each other. The same is applied to the very broad hydrogen lines, whose wings may span over two or even three spectral orders. The typical mismatch between the red and blue ends of the neighbouring orders is well within the statistical noise of these orders. The usual procedure to normalize a series of polarimetric observations of the same target, but with different angles of the retarder, is to create a sum of the individual observations, normalize it to the continuum in the way described above, and to use the master normalized image as a template for the individual observations: by taking the ratio and fitting a regular spline to it, which then finally defines the continuum surface for the individual observations.

The Stokes  $I$  and  $V$  parameters were derived following the ratio method described by Donati et al. (1997), and null polarization spectra were calculated by combining the subexposures in such a way that polarization cancels out. These steps ensure that no spurious signals are present in the obtained data (e.g. Ilyin 2012). The observing logbook is presented in Table 1, where the first column gives the date of observation, followed by the S/N ratio per resolution element of the spectra in the wavelength region around 4500 Å.

## 3 MODEL PARAMETERS AND ABUNDANCES OF HD 19400

The starting model parameters of HD 19400 were derived from Strömgren photometry. The observed colours ( $b - y$ ) =  $-0.066$ ,  $m_1 = 0.111$ ,  $c_1 = 0.512$ ,  $\beta = 2.708$  were taken from the Hauck & Mermilliod (1998) Catalogue.<sup>1</sup> The synthetic colours were taken from the grid computed for  $[M/H] = 0$  and microturbulent velocity  $\xi = 0 \text{ km s}^{-1}$  (Castelli & Kurucz 2003; Castelli & Kurucz 2006).<sup>2</sup> Zero reddening was adopted for this star, in agreement with the results from the UVBYLIST code of Moon (1985). Observed  $c_1$  and

<sup>1</sup> <http://obswww.unige.ch/gcpd/gcpd.html>

<sup>2</sup> <http://www.user.oats.inaf.it/castelli/colors/uvbybeta.html>

$\beta$  indices were reproduced by synthetic indices for model parameters  $T_{\text{eff}} = 13\,868 \pm 150$  K and  $\log g = 3.81 \pm 0.06$ , where the errors are associated with estimated errors of  $\pm 0.015$  and  $\pm 0.005$  mag for the observed  $c_1$  and  $\beta$  indices, respectively.

The parameters from the photometry were adopted for computing an ATLAS9 model with solar abundances for all the elements and zero microturbulent velocity. Using the WIDTH code (Kurucz 2005), we derived Fe II and Fe III abundances from the equivalent widths of 34 Fe II and four Fe III lines. The equivalent widths were measured with the SPLOT task of the IRAF package using the ‘e’ option, which integrates the intensity over the line profile. No Fe I equivalent widths were measured because the observed lines are weak and blended. The Fe II and Fe III abundances both satisfied the ionization equilibrium condition and provided good agreement between most of the observed and computed blended Fe I weak profiles. We did not find any trend of Fe II abundances with the excitation potential, indicating that the adopted temperature is correct. We also did not find any trend of Fe II abundances with equivalent widths, indicating that also the assumption of zero microturbulent velocity is correct. For solar abundances, the model was also able to reproduce the Balmer lines, indicating that the adopted gravity is correct.

The ATLAS9 model was used to derive the abundance for all those elements that show lines in the spectrum. Whenever possible, equivalent widths were measured. For weak and blended lines and for lines that are blends of transitions belonging to the same multiplet, such as Mg II 4481 Å, He I lines, and most O I lines, we derived the abundance from the line profiles. The synthetic spectrum was also used to determine upper abundance limits from those lines predicted for solar abundances, but not observed.

The SYNTH code (Kurucz 2005), together with line lists based mostly on Kurucz’s data (Castelli & Hubrig 2004; Castelli & Kurucz 2010; Kurucz 2011; Yüce, Castelli & Hubrig 2011) and including also data taken from the NIST data base (version 5)<sup>3</sup> were used to compute the synthetic spectrum. The synthetic spectrum was broadened both for a Gauss profile corresponding to the 115 000 resolving power of the HARPS instrument and for a rotational velocity  $v \sin i = 32$  km s<sup>-1</sup>. This value was derived from the comparison of the observed and computed profile of several lines. We estimate an uncertainty of the order of 0.5 km s<sup>-1</sup> for this choice.

Once all abundances were determined in this way, we computed an ATLAS12 model (Kurucz 2005) for the individual abundances having the same parameters as for the ATLAS9 model. However, the new ATLAS12 model did not reproduce either the Fe II–Fe III equilibrium or the hydrogen lines. In fact, the non-solar abundances of several elements, and in particular the helium underabundance, altered the model structure in a consistent way. We therefore searched for the ATLAS12 model adequate to assure the Fe II–Fe III ionization equilibrium and the Balmer lines reproducibility. We found that the ATLAS12 model with parameters  $T_{\text{eff}} = 13\,500$  K and  $\log g = 3.9$  met these requirements. The comparison between the computed H $\gamma$  profile and the H $\gamma$  profile observed in the FORS 1 spectrum at a resolution of  $\sim 2000$  on 2003 August 1 (ESO Prg. 71.D-0308(A)) is presented in Fig. 1.

The abundances  $\log(N_{\text{elem}}/N_{\text{tot}})$  of HD 19400 derived from the ATLAS12 model either from equivalent widths or line profiles are listed in Table 2, together with the solar abundances taken from Asplund et al. (2009). Similar to previous spectroscopical studies of HD 19400, no lines belonging to the secondary were detected in the three HARPS spectra. All the lines and atomic data used for the abundance analysis are listed in Table 3.

<sup>3</sup> <http://www.nist.gov/pml/data/asd.cfm>

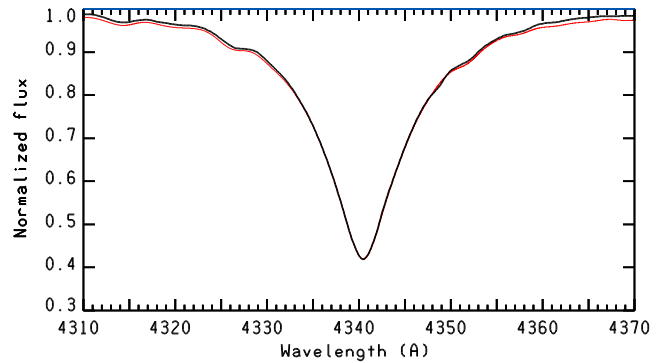


**Figure 1.** Comparison of the H $\gamma$  profile observed in the low-resolution FORS 1 spectrum (thick line) with that computed using the ATLAS12 model with parameters  $T_{\text{eff}} = 13\,500$  K and  $\log g = 3.9$  (thin line).

The most overabundant element is Xe ([+5.22]), followed by Hg ([+4.75]), Ga ([+3.97]), P ([+2.24]), Mn ([+1.71]), Fe ([+0.73]), and Ti ([+0.67]). The elements Ne, Si, Ca, and Cr are marginally overabundant. We note that a nearly solar abundance of  $-4.45$  dex, rather than the average value of  $-4.37$  dex derived from the equivalent widths, better reproduces with the synthetic spectrum most of the observed Si lines.

Helium is underabundant ( $\sim [-1.1]$ ), but it is difficult to state a definite abundance value, because some observed profiles cannot be fitted by the computed ones, whichever is the adopted abundance. These are the lines at 4026, 4387, 4471, and 4921 Å. We assumed an average abundance of  $N(\text{He})/N_{\text{tot}} = 0.007$ , which reproduces rather well most of the lines listed in Table 3. The wings of the lines at 4026, 4471, 5075, and 6678 Å are rather well reproduced by an average abundance of  $-2.17$  dex derived from all the He I lines, but the observed core is weaker than the computed one. This kind of behaviour, common to several HgMn stars (e.g. Castelli & Hubrig 2004), is ascribed to vertical abundance stratification. The whole line at 4388 Å and the red wing of the line at 4922 Å cannot be fitted. The cause could be due to the several blends affecting them. The other He I lines at 3867, 4009, 4121, 4713, 5015, and 5047 Å are well reproduced by the  $-2.17$  dex abundance. Some of them have minor contributions of blends.

Other underabundant elements are Al ( $\leq [-1.2]$ ), S ( $[-1.1]$ ), O ( $[-0.69]$ ), C ( $[-0.60]$ ), and Mg ( $[-0.60]$ ). Finally, Ni is marginally underabundant.

We could identify a few observed but not predicted lines as As II. In fact, no As II lines are included in our line list owing to the lack of  $\log gf$  values and excitation potentials for them. We used As II wavelengths listed in the NIST data base to identify the lines observed at 4494.30, 5497.727, 5558.09, 5651.32, and 6170.27 Å as due to As II. Arsenic was reportedly also present in the HgMn stars 46 Aql (Sadakane et al. 2001) and HD 71066 (Yüce et al. 2011).

No lines of rare earth elements, as well as no lines of Y II, Pt II, and Au II were observed.

For comparison, the abundances from Alonso et al. (2003) are listed in the last column of Table 2. There is a large disagreement for almost all elements, except for silicon and iron. The differences in the abundances for iron and silicon amount to 0.05 dex for Fe II, 0.15 dex for Fe III, and 0.06 dex for Si II. They can be related with both the different ATLAS9 parameters and the microturbulent velocities adopted for the abundance analysis. The ATLAS9 parameters in this study are  $T_{\text{eff}} = 13\,870$  K,  $\log g = 3.8$ ,  $[M/H] = 0.0$ , while those of Alonso et al. (2003) are  $T_{\text{eff}} = 13\,350$  K,  $\log g = 3.76$ ,

**Table 2.** Abundances  $\log(N_{\text{elem}}/N_{\text{tot}})$  for HD 19400. For each element listed in the first column, we present the abundance computed using the ATLAS12 model in the second column. In parentheses is the number of lines adopted to derive the abundance for a given ion. Blended lines were counted only once. In the third column, we list the deviations from solar abundances (Asplund et al. 2009) presented in column 4. The last column gives the abundances derived by Alonso et al. (2003).

Element	HD 19400 [13 500 K,3.9,ATLAS12]	Star–Sun	Sun	Alonso et al. (2003) [13 350 K,3.76,ATLAS9]
He I	$-2.17 \pm 0.08$ : (14)	[−1.11]:	−1.05	−1.52
C II	$-4.12 \pm 0.02$ (4)	[−0.51]	−3.61	$-3.52 \pm 0.28$
O I	−3.90 (2)	[−0.55]	−3.35	$-3.31 \pm 0.07$
Ne I	$-3.77 \pm 0.07$ (6)	[+0.34]	−4.11	
Na I	−5.71 (2)	[+0.09]	−5.80	
Mg II	−5.06 (4)	[−0.62]	−4.44	$-4.65 \pm 0.30$
Al II	$\leq -6.77$ (2)	$\leq [-1.18]$	−5.59	
Si II	$-4.36 \pm 0.17$ (10)	[−0.17]	−4.53	$-4.28 \pm 0.31$
Si III	$-4.37 \pm 0.02$ (2)	[−0.16]	−4.53	
P II	$-4.26 \pm 0.15$ (33)	[+2.28]	−6.63	$-5.95 \pm 0.16$
P III	$-4.44 \pm 0.09$ (4)	[+2.19]	−6.63	
S II	−5.82 (1)	[−0.90]	−4.90	$-5.07 \pm 0.47$
Ca II	−5.50: (1)	[+0.20]:	−5.70	
Ti II	$-6.35 \pm 0.07$ (9)	[+0.74]	−7.09	$-5.69 \pm 0.37$
Cr II	$-6.24 \pm 0.09$ (5)	[+0.16]	−6.40	$-5.45 \pm 0.42$
Mn II	$-4.94 \pm 0.18$ (6)	[+1.67]	−6.61	$-4.57 \pm 0.33$
Fe II	$-3.79 \pm 0.14$ (35)	[+0.75]	−4.54	$-3.75 \pm 0.31$
Fe III	$-3.82 \pm 0.10$ (4)	[+0.72]	−4.54	$-3.67 \pm 0.30$
Ni II	−5.84 (1)	[−0.02]	−5.82	$-5.51 \pm 0.34$
Ga II	$-5.19 \pm 0.17$ (12)	[+3.81]	−9.00	
Sr II	−9.07 (1)	[+0.10]	−9.17	$-6.95 \pm 0.38$
Xe II	$-4.65 \pm 0.17$ (6)	[+5.15]	−9.80	
Hg II	$-6.16 \pm 0.13$ (3)	[+4.71]	−10.87	−4.43

**Table 3.** Line by line abundances of HD 19400 from the ATLAS12 model with parameters  $T_{\text{eff}} = 13\,500$  K,  $\log g = 3.9$ . In the second and third columns, we give the oscillator strength with the corresponding data base source. The low-excitation potential is listed in column 4, followed by the equivalent width and the derived abundance. For a number of lines, the abundance was derived from line profiles. The full table is available online.

$\lambda(\text{\AA})$	HD 19400[13 500,3.9,ATLAS12]			$W(\text{m}\text{\AA})$	$\log(N_{\text{elem}}/N_{\text{tot}})$	Remarks
	$\log gf$	Ref. <sup>a</sup>	$\chi_{\text{low}}$			
$\log(N(\text{He I})/N_{\text{tot}}) = -2.17 \pm 0.08$ :						
3867.4723	−2.038	NIST5	169 086.766	Profile	−2.155	
3867.4837	−2.260	NIST5	169 086.843	Profile	−2.155	
3867.6315	−2.737	NIST5	169 087.631	Profile	−2.155	
4009.2565	−1.447	NIST5	171 134.897	Profile	−2.155	
4026.1844	−2.628	NIST5	169 086.766	Profile	−2.155::	No fit
4026.1859	−1.453	NIST5	169 086.766	Profile	−2.155::	
4026.1860	−0.704	NIST5	169 086.766	Profile	−2.155::	
4026.1968	−1.453	NIST5	169 086.843	Profile	−2.155::	
4026.1983	−0.976	NIST5	169 086.843	Profile	−2.155::	

$[M/H] = 0.5$ ; the microturbulent velocities are  $\xi = 0.0$  km s<sup>−1</sup> and 1.2 km s<sup>−1</sup>, respectively. However, the differences for all the other elements are too large to be only due to the different choices for the parameters. Furthermore, Alonso et al. (2003) derived abundances for numerous elements that we did not observe at all in our spectra, while we identified and derived abundances for Ne I, Ga II, and Xe II that were not mentioned at all by Alonso et al. (2003), although these elements are present with numerous lines. Unfortunately, they did not publish the list of lines and equivalent widths they used, so that any further comparison is not possible.

The ATLAS12 model was preferred to ATLAS9 for final abundance determination, to ensure consistency with the SYNTH code in computing the line profiles; however, abundance values derived

using ATLAS9 and ATLAS12 differ by no more than 0.05 dex. The observed and synthetic spectra are presented on F. Castelli’s web page<sup>4</sup> together with the line-by-line identification.

### 3.1 Emission lines

Similar to the spectral behaviour of a number of HgMn stars, the lines of multiplet 13 of Mn II ( $\lambda\lambda$  6122–6132 Å) appear to be affected by emission. In fact, a very weak emission is observed for the blends

<sup>4</sup> <http://wwwuser.oats.inaf.it/castelli/hd19400/hd19400.html>

$\lambda\lambda$  6125.861, 6126.225 Å, while a well-observable strong absorption is predicted at these wavelengths. Furthermore, the blends at  $\lambda\lambda$  6122.432, 6122.807 Å, at 6128.726, 6129.019, 6129.237 Å, and at 6130.793, 6131.011, 6131.918 Å are observed much weaker than computed, so that the core could have been filled by emission.

Other CP stars showing this kind of emission are, for example, 3 Centauri A (Sigut, Landstreet & Shorlin 2000), (Wahlgren & Hubrig 2004), 46 Aquilae (Sigut et al. 2000), HR 6000 (Castelli & Hubrig 2007), and HD 71066 (Yüce et al. 2011). This phenomenon was explained either in the context of non-LTE line formation (Sigut 2001) or as due to a possible fluorescence mechanism (Wahlgren & Hubrig 2000).

### 3.2 Anomalous line profile shapes

In all HARPS spectra, the lines of Mn II and Hg II present anomalous flat-bottom line profiles reminiscent of profile shapes observed in numerous HgMn stars (e.g. Hubrig et al. 2006b, 2011; Makaganiuk et al. 2011b), while the lines of other elements exhibit typical rotationally broadened line profiles. As an example, we display in Fig. 2 the average Mn II profile overplotted with the average Fe II profile, using the best almost blend-free lines of moderate strength. To construct the average Mn II profile, we employed the Mn II lines  $\lambda\lambda$ 4292.2, 4363.3, 4478.6, 4518.9, 4738.3, 4755.7, and 4764.7. Three of them,  $\lambda\lambda$ 4738.3, 4755.7, and 4764.7, have not been used in the abundance analysis because of their unknown hyperfine structure. We note that two more Mn II lines,  $\lambda\lambda$ 4206.4 and 4365.2, were employed in the abundance analysis (see Table 3). They are not included in our sample of lines selected for the search of variability, as the line at  $\lambda\lambda$ 4206.4 is slightly disturbed by a blend in the blue wing and the weak line at  $\lambda\lambda$ 4365.2 is considerably affected by noise at the third epoch. In the calculation of the average Fe II profile, we used the Fe II lines  $\lambda\lambda$ 4122.7, 4296.6, 4491.4, 4522.6, 4923.9, 5002.0, and 5061.7, which constitute a subset of the sample of Fe II lines employed in the Fe abundance determination.

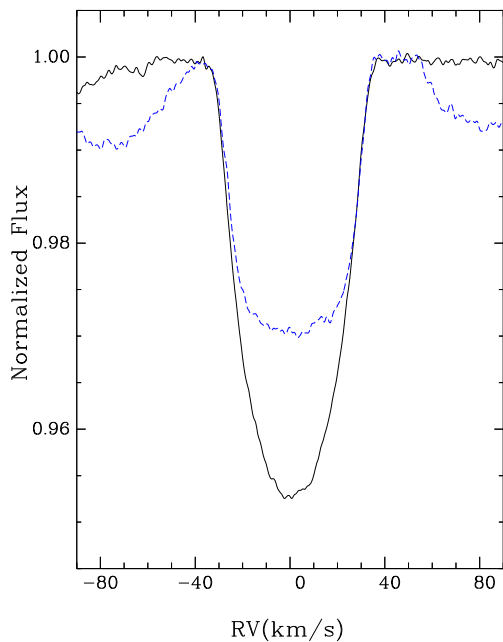


**Figure 2.** Comparison of the average Mn II line profile (dashed line) with the average Fe II line profile (solid line).

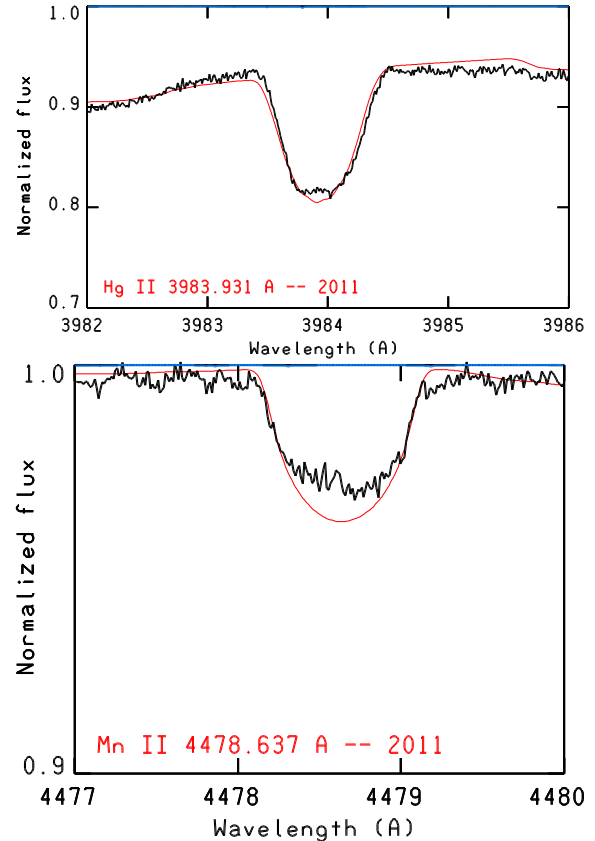


**Figure 3.** Hg II and Mn II line profiles observed in the HARPSpol spectrum obtained in 2011 highlighted in black together with the synthetic profile shown by the thin red line. The shape of the line profiles belonging to Hg II and Mn II deviates from the purely rotationally broadened profiles observed in the Fe II and Cr II lines, indicating an inhomogeneous distribution of Hg and Mn on the stellar surface.

The calculation of the synthetic spectrum for individual Mn II and Hg II lines indicates that the anomalous flat-bottom line profile shape is not caused by the presence of isotopic/hyperfine structure. In the top panel of Fig. 3, we display the synthetic profile of the Hg II  $\lambda$ 3984 line overplotted with the observed line profile. The bottom panel presents the synthetic and observed profiles of the Mn II  $\lambda$ 4478 line. The observed anomalous profile shape of both lines is reminiscent of the behaviour of line profiles of various elements in typical HgMn stars (e.g. Hubrig et al. 2006b). In spectroscopic binaries, these elements are frequently concentrated in non-uniform equatorial bands, which disappear exactly on the surface area, which is permanently facing the secondary (e.g. Hubrig et al. 2010).

## 4 SPECTRAL VARIABILITY

For the study of the spectral variability, we have on our disposal two HARPS spectra taken on two consecutive nights in 2011 December, while the third HARPS spectrum was obtained in 2013 July. The spectra have different quality with a S/N of about 800 for observations in 2011 and a S/N of only about 500 for the observation in 2013. To better understand the chemical spot pattern on the surface of HD 19400, we decided to analyse the spectral variability by the comparison of observations separated by two time-scales. On the one hand, we compared the spectra from 2011 with each other to study the day-to-day variations, and on the other hand, we compared

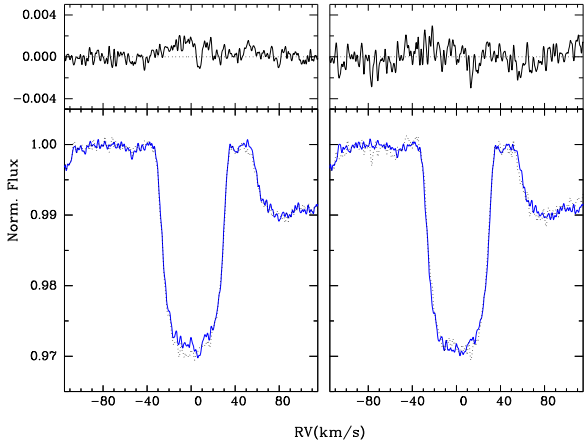


**Figure 4.** Profile variations of the Mn lines. Left-hand panel: day-to-day variations; solid and dotted lines correspond to 2011 December 15 and 16, respectively. Right-hand panel: year-to-year variations; solid and dotted lines present 2011 and 2013 observations, respectively. The upper part of each panel shows the difference between the two plotted spectra.

the spectrum obtained in 2013 against the average of the two spectra from 2011 to search for long-term variation in the line profiles.

In the left-hand panel of Fig. 4, we compare the mean Mn II profiles obtained on two nights in 2011. In the difference spectrum, the rms of the noise in the nearby continuum is about 0.05 per cent while the variations are about 0.15 per cent. The variability of the Mn lines is detected therefore at a level of  $3\sigma$ . We note that if the high-frequency noise is filtered, it becomes evident that the observed day-to-day variation is in fact four times larger than the  $\sigma$  of the noise of similar frequency. The year-to-year variations are apparently not larger than the day-to-day variations, and, since the S/N of the spectrum obtained in 2013 is lower, the variations between 2011 and 2013 are not so clear. The flux differences, however, are still present at a level of about  $2\sigma$ .

The same procedure as for the study of the Mn lines was applied to the Fe lines. Fig. 5 shows the mean profile of the seven Fe lines. The day-to-day flux variations within the line profile are on the order of 0.13 per cent, which is three times larger than the noise and of the order of  $4\sigma$ , if high frequencies are filtered. Year-to-year

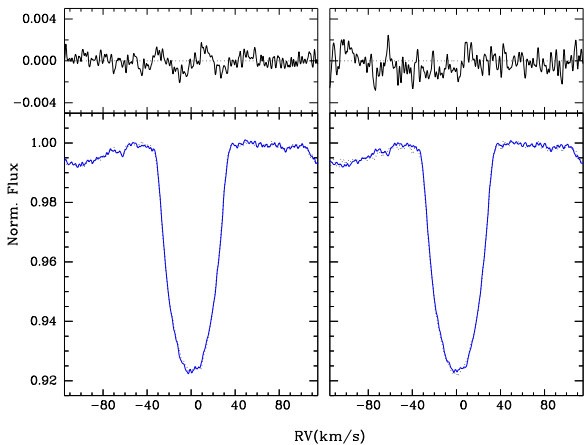


**Figure 5.** Profile variations of the Fe lines. Left-hand panel: day-to-day variations; solid and dotted lines correspond to 2011 December 15 and 16, respectively. Right-hand panel: year-to-year variations; solid and dotted lines present 2011 and 2013 observations, respectively. The upper part of each panel shows the difference between the two plotted spectra.

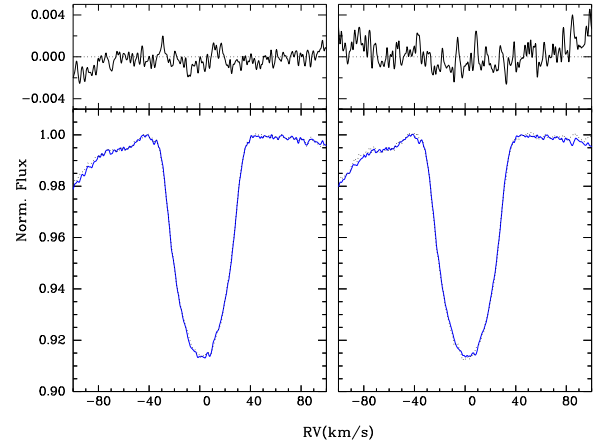


**Figure 6.** Profile variations of the P lines. Left-hand panel: day-to-day variations; solid and dotted lines correspond to 2011 December 15 and 16, respectively. Right-hand panel: year-to-year variations; solid and dotted lines present 2011 and 2013 observations, respectively. The upper part of each panel shows the difference between the two plotted spectra.

flux differences are similar in size, but in this case represent only a level of about 1.5 times over the noise and  $\sim 2\sigma$ , after filtering high frequencies.

To study the variability of the P II lines, we selected the following six blend-free P II lines:  $\lambda\lambda 4420.71, 4530.82, 4589.85, 5386.90, 6024.18,$  and  $6043.08$ . The line profile difference between the two spectra taken in 2011 resembles that of the Fe lines (Fig. 6). However, the noise in this case is higher and the detection would be only at a level of  $2\sigma$ . The year-to-year comparison shows no significant variation, probably due to the rather high noise level.

The behaviour of line profiles belonging to other elements with strong overabundances, in particular Hg and Ga, also indicates a non-uniform distribution. Unfortunately, for these elements, the number of useful lines is low and consequently the detection threshold is higher. Fig. 7 shows the differences between the spectra around the only two clean Ga lines:  $\lambda 4254.0$  and  $\lambda 4255.7$ . We note that the shape difference in the line profiles between spectra obtained on 2011 December 15 and 16 is the same for both Ga lines. This supports the genuineness of the variation behaviour, even if the

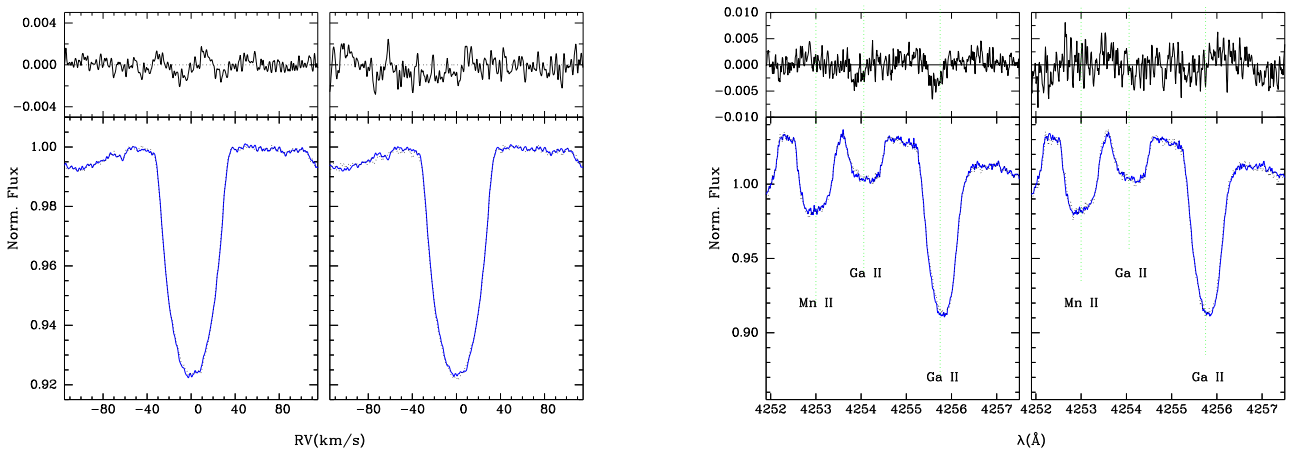


**Figure 7.** Profile variations of the Ga lines. Left-hand panel: day-to-day variations; solid and dotted lines correspond to 2011 December 15 and 16, respectively. Right-hand panel: year-to-year variations; solid and dotted lines present 2011 and 2013 observations, respectively. The upper part of each panel shows the difference between the two plotted spectra.

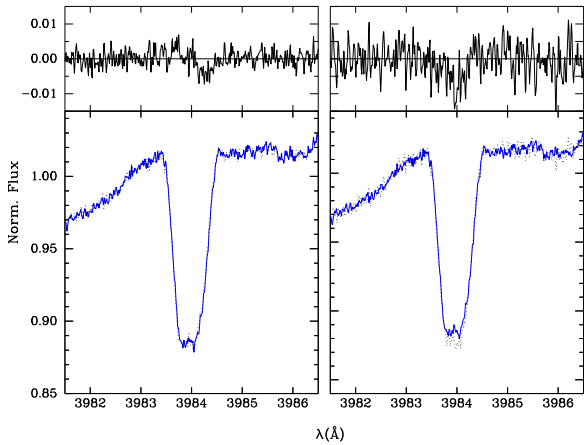


**Figure 8.** Profile variations of the Hg line. Left-hand panel: day-to-day variations; solid and dotted lines correspond to 2011 December 15 and 16, respectively. Right-hand panel: year-to-year variations; solid and dotted lines present 2011 and 2013 observations, respectively. The upper part of each panel shows the difference between the two plotted spectra.

flux differences are not larger than  $2\sigma$ . The differences with respect to the 2013 spectrum are within the noise level.

It is a remarkable finding that the Ga II lines appear indicative of variability. Previous studies of He-weak magnetic Bp stars with similar atmospheric parameters and with well-established strong magnetic fields also indicated strong overabundances of P, Ga, Xe, and a few heavy elements, such as Pt and Hg (e.g. Collado & Lopez-Garcia 2009). Furthermore, a number of magnetic Bp stars with strongly overabundant Ga display a large variation of Ga lines, which become the strongest at longitudinal magnetic field maxima, suggesting that Ga is accumulating near the magnetic poles (e.g. Artru & Freire-Ferrero 1988). Interestingly, Alecian & Artru (1987) presented the radiative accelerations of gallium in Bp star atmospheres and concluded that the presence of a magnetic field strongly modifies the gallium accumulation.

Also the Hg line at 3984 Å presents noticeable variations (Fig. 8). Day-to-day variations are of the order of 0.4 per cent, while differences of about 0.8 per cent are present between the 2011 and 2013 observations. In both cases, the variation is at a  $2\sigma$  level. If high frequencies are filtered, then the variations are at a  $3\text{--}4\sigma$  level.

Due to the small number of available spectra, it is currently not possible to decide whether the variability pattern of the line profiles belonging to different elements can be explained by an inhomogeneous element distribution on the stellar surface, or is due to pulsations. Although no information on the rotational period is given in the literature, its upper limit can be estimated from the measured  $v \sin i$ -value and the stellar radius. Using  $v \sin i = 32.0 \pm 0.5 \text{ km s}^{-1}$  and  $R = 3.7 \pm 0.5 R_{\odot}$  calculated using main-sequence evolutionary CLÉS models (Scuflaire et al. 2008), we obtain an upper limit of  $P \leq 5.85 \pm 0.8 \text{ d}$ . It is clear that with such a rather low value for the rotation period, one can already expect to see weak variability in observations obtained on two consecutive nights.

In Fig. 9, we show the position of HD 19400 in the  $\log T_{\text{eff}}\text{--}\log g$  diagram together with the boundaries of the theoretical instability strips calculated for different metallicities ( $Z = 0.01$  and  $Z = 0.02$ ) and using the OP opacities (<http://cdsweb.u-strasbg.fr/topbase/op.html>, see also Miglio et al. 2007). The PGa star HD 19400 with  $T_{\text{eff}} = 13\,500 \text{ K}$  and  $\log g = 3.90$  falls well inside the classical instability strip, where slowly pulsating B-type stars are found with expected pulsation periods from several hours

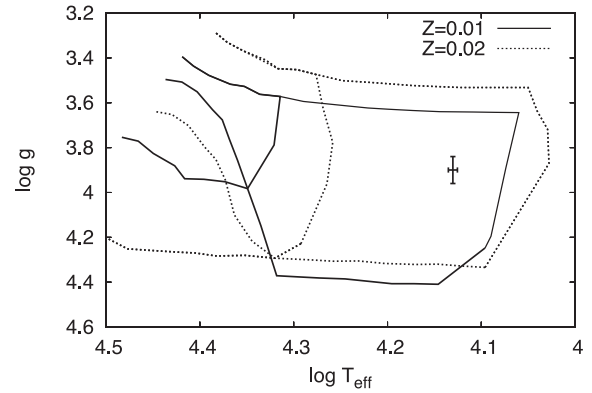


**Figure 9.** The position of the PGa star HD 19400 in the H–R diagram. The boundaries of the theoretical instability strips for  $\beta$  Cep and SPB stars are taken from Miglio, Montalbán & Dupret (2007) for OP opacities. Full lines correspond to strips for metallicity  $Z = 0.01$  and dotted lines to strips with metallicity  $Z = 0.02$ .

to a few days. Also classical magnetic Bp stars are located in the same region of the H–R diagram and frequently display strong overabundances of P, Ga, Xe, and heavy elements.

Since polarimetric observations usually consist of a number of short subexposures taken at different angles of the retarder wave plate, we used all available Stokes  $I$  spectra for each subexposure to search for the presence of short-term variations in Mn and Hg line profiles. During both nights in 2011 December, the time difference between individual subexposures accounts for 13 min, while it is about 20 min for the observations in 2013 July. In Fig. 10, we present the behaviour of line profiles of the Hg II  $\lambda 3984$  line, and the Mn II  $\lambda 4478$  line, in HARPSpol subexposures obtained on 2011 December 15 and 16 and on 2013 July 19. No notable line profile variations above the noise level, which is about 0.22 per cent of the continuum flux in the 2011 spectra and about 0.32 per cent in 2013, are detected on these time-scale.

## 5 MAGNETIC FIELD

A few polarimetric spectra of HD 19400 were previously obtained with FORS 1 (Hubrig et al. 2006a), and most recently with FORS 2 on Antu (UT1) from 2011 May to 2012 January (Hubrig et al. 2012) at the rather low resolution of  $\sim 2000$ . The magnetic field measurements from these earlier data are presented in Table 4 together with the modified Julian date of mid-exposure. Out of the three measurements, weak magnetic field detections at a  $3\sigma$  significance level were achieved on two different epochs. Given the low resolution of FORS 1/2, these spectra do not however allow us to measure the longitudinal magnetic field on lines of individual elements separately.

We note that the magnetic field topology in HgMn stars is currently unknown. The recent study of Hubrig et al. (2012) seems to indicate the existence of intriguing correlations between the strength of the magnetic field, abundance anomalies, and binary properties. Measurement results for a few stars revealed that element underabundance (respectively, overabundance) is observed where the polarity of the magnetic field is negative (respectively, positive). An inhomogeneous chemical abundance distribution is observed most frequently on the surface of upper-main-sequence Ap/Bp stars with large-scale organized magnetic fields. The abundance distribution of certain elements in these stars is usually non-uniform and non-symmetric with respect to the rotation axis, but shows a kind of

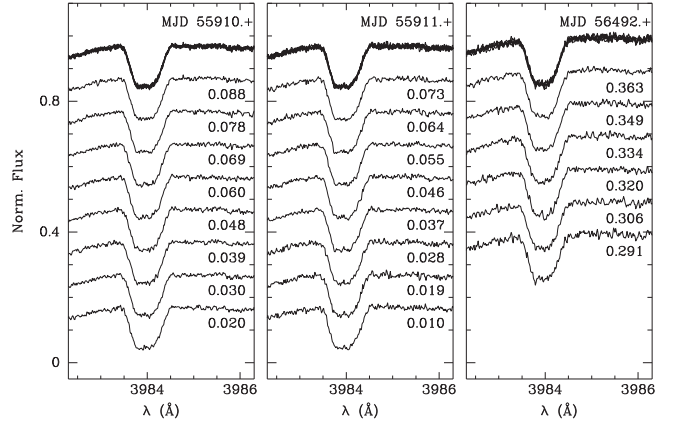
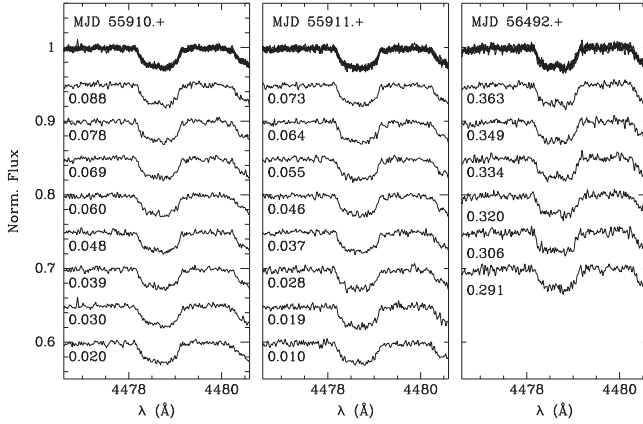


**Figure 10.** The behaviour of the line profiles of the Mn II  $\lambda 4478$  line (left-hand panel) and the Hg II  $\lambda 3984$  line (right-hand panel) in HARPSpol subexposures obtained on 2011 December 15 and 16, and on 2013 July 19. The overlotted profiles are presented on the top.

**Table 4.** Previous magnetic field measurements of HD 19400 using FORS 1/2. In the first column, we list the modified Julian date of mid-exposure followed by the measurements of the mean longitudinal magnetic field  $\langle B_z \rangle_{\text{all}}$  using all available spectral lines and  $\langle B_z \rangle_{\text{hyd}}$  using only hydrogen lines. All quoted errors are  $1\sigma$  uncertainties.

MJD	$\langle B_z \rangle_{\text{all}}$ [G]	$\langle B_z \rangle_{\text{hyd}}$ [G]
52852.371	$151 \pm 46$	$217 \pm 65$
55845.295	$14 \pm 24$	$32 \pm 26$
55935.109	$-65 \pm 26$	$-110 \pm 30$

symmetry between the topology of the magnetic field and the element distribution. Assuming that a similar kind of symmetry exists in HgMn and PGa stars, it appears reasonable to use the Mn II lines for magnetic field measurements since Mn II shows the strongest variability in the spectra of HD 19400.

The major problem in the analysis of high-resolution spectra is the proper line identification of blend free spectral lines. The quality of the selection varies strongly from star to star, depending on binarity, line broadening, and the richness of the spectrum. The best 22, mostly blend-free, Mn II lines, including also six Mn II lines used in the abundance determination, we employed in the diagnosis of the magnetic field on the surface of HD 19400 are presented in Table 5 together with their Landé factors. The Landé factors were taken from Kurucz's list of atomic data.<sup>5</sup> As a first step, we used for the measurements the moment technique developed by Mathys (e.g. Mathys 1991). This technique allows us not only the determination of the mean longitudinal magnetic field, but also to prove the presence of crossover effect and quadratic magnetic fields. For each line, the measured shifts between the line profiles in the left- and right-hand circularly polarized HARPS spectra are presented in Table 5. The linear regression analysis in the  $\Delta\lambda$  versus  $\lambda^2 g_{\text{eff}}$  diagram, following the formalism discussed by Mathys (1991, 1994), yields values for the mean longitudinal magnetic field  $\langle B_z \rangle$  between  $-70$  G and  $+65$  G. A weak negative longitudinal magnetic field  $\langle B_z \rangle = -70 \pm 23$  G at  $3\sigma$  level is measured on the first epoch, and  $\langle B_z \rangle = 65 \pm 30$  G at  $2.2\sigma$  level on the third epoch.

**Table 5.** Shifts between the line centres of gravity in the right and left circularly polarized spectra obtained on three different nights. In the first column, we list the wavelengths of the Mn II lines followed by their corresponding Landé factors and the wavelength shifts in  $\text{\AA}$  on each epoch.

$\lambda$ [ $\text{\AA}$ ]	$g_{\text{eff}}$	$\Delta\lambda$ [ $\text{\AA}$ ]		
		Night 1	Night 2	Night 3
4000.033	1.076		0.0001	0.0014
4110.615	1.002	-0.0010	0.0004	
4184.454	1.065	-0.0024	-0.0005	
4206.367	1.362	-0.0001	0.0020	-0.0013
4240.390	0.929	-0.0046	0.0040	0.0024
4259.200	1.315	-0.0009	-0.0016	-0.0013
4260.467	2.725	-0.0027	0.0040	0.0086
4292.237	1.270	-0.0001		0.0051
4326.639	1.379	-0.0013	0.0004	0.0011
4363.255	1.112	-0.0019	-0.0005	0.0043
4365.217	1.500		-0.0042	0.0067
4478.637	1.500	-0.0104	0.0026	
4518.956	1.507	-0.0007	-0.0013	
4727.841	0.506		0.0031	0.0029
4730.395	0.712	0.0022	-0.0022	
4734.136	0.724	-0.0010		
4738.290	1.080	0.0005		
4755.727	1.058	-0.0029	0.0009	
4764.728	1.027	-0.0009	0.0019	0.0032
4791.782	1.085	-0.0076	-0.0042	-0.0030
4806.823	1.048	0.0013	0.0028	
4839.737	1.358	-0.0031	-0.0027	0.0090

Further, the mean longitudinal magnetic fields  $\langle B_z \rangle_{\text{Mn},N}$  were measured from null polarization spectra, which are calculated by combining the subexposures in such a way that polarization cancels out. The results of our measurements are presented in Table 6, and the corresponding linear regression plots are shown in Fig. 11. The measurements on the spectral lines of Mn II using null spectra are labelled by  $N$  in Table 6. Since no significant fields could be determined from null spectra, we conclude that any noticeable spurious polarization is absent. No significant crossover and mean quadratic magnetic field have been detected on the three observing epochs.

Our assumption that the inhomogeneous distribution of Mn II over the stellar surface is due to the action of a magnetic field does not exclude the possibility that also ions with less pronounced line profile variability are inhomogeneously distributed across the stellar

<sup>5</sup> <http://kurucz.cfa.harvard.edu/atoms>

**Table 6.** Magnetic field measurements of HD 19400 using HARPS. In the first column, we list the modified Julian date of mid-exposure followed by the measurements of the mean longitudinal magnetic field using Mn II lines from polarized spectra and null polarization spectra. All quoted errors are  $1\sigma$  uncertainties.

MJD	$\langle B_z \rangle_{\text{Mn}}$ [G]	$\langle B_z \rangle_{\text{Mn, N}}$ [G]
55910.054	$-70 \pm 23$	$-13 \pm 24$
55911.042	$28 \pm 18$	$-18 \pm 21$
56492.327	$65 \pm 30$	$25 \pm 32$

surface. Indeed, they could be concentrated towards the rotation poles, or have a predominantly symmetric distribution about the rotation axis. Among the elements showing less pronounced line profile variations in the spectra, the most numerous lines belong to Fe II and P II. Additional magnetic field measurements have been thus carried out using 35 Fe II and 33 P II lines listed in Table 3. Neither measurements using the Fe II lines nor the P II lines showed evidence for the presence of a magnetic field.

During the last few years, a number of attempts to detect mean longitudinal magnetic fields in HgMn stars have been made by several authors using the line addition technique, the least-squares deconvolution (e.g. Makaganiuk et al. 2011a,b), and the multiline Singular Value Decomposition (SVD) technique (Hubrig et al. 2014). A high level of precision, from a few to tens of Gauss, is achieved through application of these techniques (Donati et al. 1997; Carroll et al. 2012), which combine hundreds of spectral lines of various elements. In such techniques, an assumption is made that all spectral lines are identical in shape and can be described by a scaled mean profile. However, the lines of different elements with different abundance distributions across the stellar surface sample the magnetic field in different manners. Combining them, as is done with such techniques, may lead to the dilution of the magnetic signal or even to its (partial) cancellation, if enhancements of different elements occur in regions of opposite magnetic polarities. A shortcoming of both techniques is that a high level of precision is achievable only if a large number of lines is involved in the analysis.

In Fig. 12, we present the results of the SVD analysis of the observations on all three epochs using 32 Mn II lines selected from the VALD data base (e.g. Piskunov et al. 1995; Kupka et al. 2000). We note that although the S/N of the two data sets obtained in 2011 is higher than for the most recent observation, the reconstruction for the last observation was performed with a smaller number of

eigenprofiles, which results in a smaller relative noise contribution. As the noise level scales with the effective dimension of the signal subspace (see section 3 of Carroll et al. 2012), the noise levels of the reconstructed profiles for all three nights are approximately the same. On the first epoch, the measurement using the SVD technique shows the longitudinal magnetic field  $\langle B_z \rangle = -76 \pm 25$  G. Using the false alarm probability (FAP; Donati, Semel & Rees 1992) in the region of the whole Stokes  $I$  line profile, we obtain for this measurement  $\text{FAP} = 0.008$ . According to Donati et al. (1992), an FAP smaller than  $10^{-5}$  can be considered as definite detection, while  $10^{-5} < \text{FAP} < 10^{-3}$  are considered as marginal detections. We note that at this epoch the Zeeman feature is well visible in the Stokes  $V$  spectrum. However, the obtained FAP value is too high for a marginal detection. The interesting fact is that the observed Stokes  $V$  Zeeman feature is slightly shifted to the blue from the line centre.

For the second epoch, we measure the mean longitudinal magnetic field  $\langle B_z \rangle = 9 \pm 35$  G with the corresponding FAP value of 0.045. The observed Zeeman feature in the SVD Stokes  $V$  profile is reminiscent of a typical crossover profile, and, similar to the Zeeman feature in the first epoch, is also slightly shifted to the blue from the line centre. The corresponding FAP values are 0.045 for the second epoch and 0.25 for the third epoch. Especially intriguing is the appearance of the SVD Stokes  $I$  profile with the corresponding Zeeman feature in the SVD Stokes  $V$  profile obtained for the third epoch. The shape of the SVD Stokes  $I$  profile shows a slight splitting shifted from the line centre, indicating that we likely observe in this phase two Mn surface spots. If we assume that the Zeeman feature in the SVD Stokes  $V$  profile is not due to pure noise, then the observed negative and positive peaks in the Zeeman feature could probably correspond to two different Mn spots. The measured field for these features indicates a magnetic field of about  $-35$  G for the negative peak and  $+35$  G for the positive peak with  $\text{FAP} = 0.029$ . On the other hand, it is clear that the amplitude of the features inside the SVD profiles is comparable to the amplitude of the noise outside the SVD profiles.

A similar analysis using the SVD technique was carried out for 115 Fe II and 33 P II lines selected from the VALD data base. The measurement on the first epoch using Fe II shows a longitudinal magnetic field  $\langle B_z \rangle = -91 \pm 35$  G with a false alarm probability  $\text{FAP} = 0.003$ . For the second epoch, we obtained  $\langle B_z \rangle = -28 \pm 21$  G with  $\text{FAP} = 0.009$ . No indications for a probable presence of a weak magnetic field was found on the third epoch. The obtained FAP value for the measurement on the first epoch is lower than that obtained for the measurement on the Mn II lines, but is still three times too high for a marginal detection.

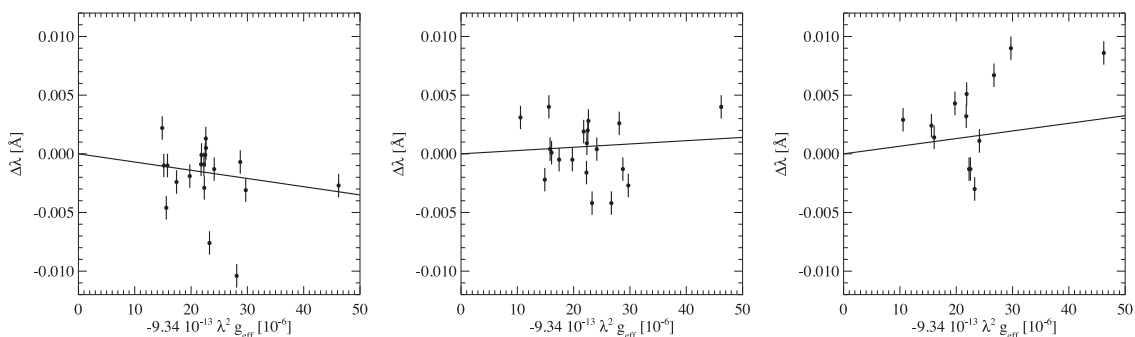


**Figure 11.** Linear regression analysis applied to the observations on three different nights. For each line, the shift between the line centres of gravity in the right and left circularly polarized spectra is plotted against  $-9.3410^{-13}\lambda_{\text{eff}}^2$ . The straight lines represent the best-fitting resulting from a linear regression analysis.

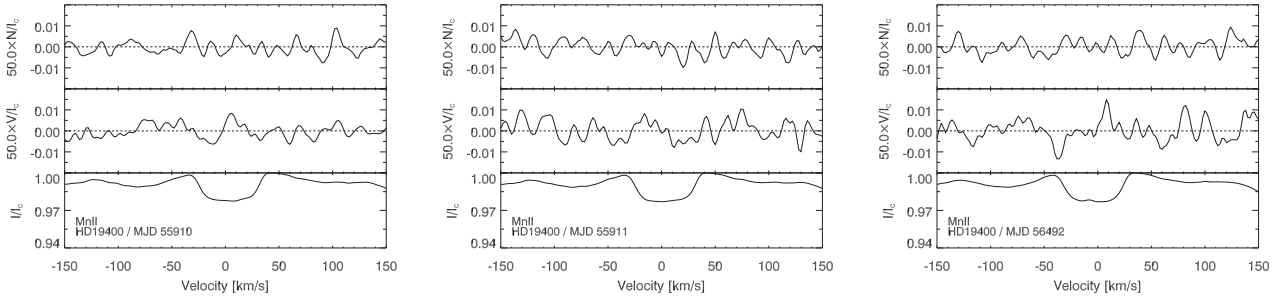


**Figure 12.** From left to right, we present the Mn II SVD profiles of HD 19400 obtained at the three different epochs from polarized spectra and null polarization spectra. From bottom to top, one can see the  $I$ ,  $V$ , and  $N$  profiles. The  $V$  and  $N$  profiles were expanded by a factor of 50 for better visibility.

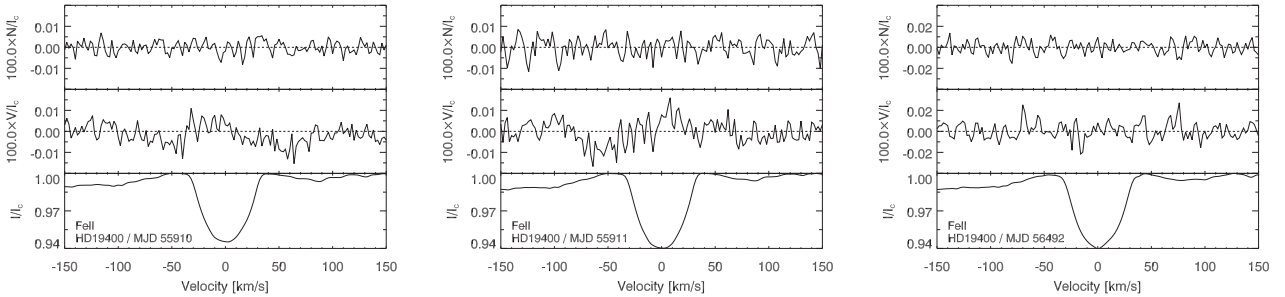


**Figure 13.** From left to right, we present the Fe II SVD profiles of HD 19400 obtained at the three different epochs from polarized spectra and null polarization spectra. From bottom to top, one can see the  $I$ ,  $V$ , and  $N$  profiles. The  $V$  and  $N$  profiles were expanded by a factor of 100 for better visibility.

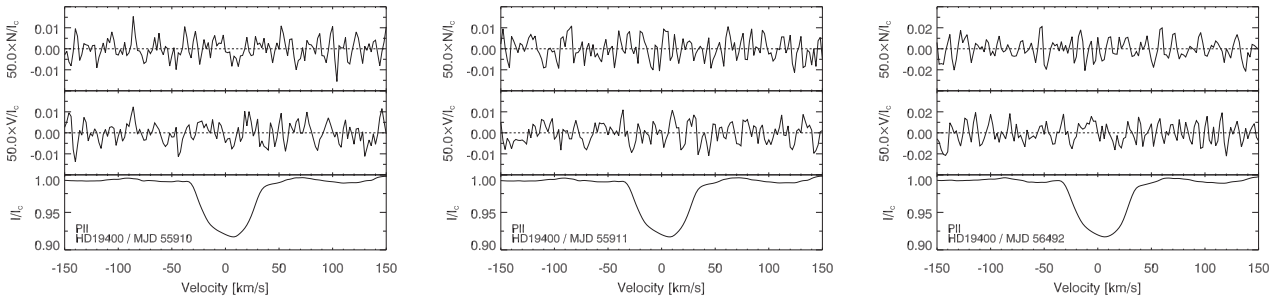


**Figure 14.** From left to right, we present the P II SVD profiles of HD 19400 obtained at the three different epochs from polarized spectra and null polarization spectra. From bottom to top, one can see the  $I$ ,  $V$ , and  $N$  profiles. The  $V$  and  $N$  profiles were expanded by a factor of 50 for better visibility.

No field detection was achieved in the analysis using the P II lines, where the Stokes  $V$  spectra appear rather flat on all three epochs. In Figs 13 and 14, we present the results of the SVD analysis using the Fe II and P II lines, respectively.

In summary, although some indications on the probable existence of a weak magnetic field in HD 19400 are found in our analysis, no definite conclusion on the presence of the magnetic field and its topology can currently be drawn. Obviously, more high-resolution, high S/N polarimetric observations are urgently needed to properly understand the nature of this type of stars.

## 6 DISCUSSION

In this work, we used high quality HARPSpol spectra of the PGa star HD 19400 to carry out an abundance analysis, search for spectral variability, and the presence of a weak magnetic field. We present the abundances of various elements determined using an ATLAS12

model, including the abundances of a number of elements not analysed by previous studies. We also report on the first detection of anomalous shapes of line profiles belonging to Mn and Hg. We suggest that the variability of the line profiles of certain elements is caused by a non-uniform surface distribution of these elements similar to the presence of chemical spots detected in HgMn stars.

One important task for future studies is to obtain detailed information on the pulsation behaviour of spectral lines in a few PGa stars by monitoring the behaviour of line profiles based on high-quality spectroscopic time series over several hours using short exposures of the order of minutes. Current stellar models do not predict non-radial pulsations of the order of 5–20 min in mid B-type stars similar to those detected in roAp stars. On the other hand, such pulsations were not originally predicted for roAp stars either. In roAp stars, the pulsation variability is best detected in the line profiles of doubly ionized rare earth elements that build element clouds in high atmospheric layers. In close parallel to roAp

stars, a theoretical consideration of B-type stars with Hg and Mn overabundances suggest that these elements can be concentrated in high-altitude clouds (above  $\log \tau = -4$ ; e.g. Michaud, Reeves & Charland 1974; Alecian, Stift & Dorfi 2011), with a potential effect of weak magnetic fields on their formation (e.g. Alecian 2013). Clearly, a careful investigation of the variability of mid B-type stars is of great interest to studies of stellar structure and evolution.

Our measurements of the magnetic field with the moment technique using 22 Mn II lines indicate the potential presence of a weak variable longitudinal magnetic field of the order of tens of gauss. The question of the presence of weak magnetic fields in stars with Hg and Mn overabundances is still under debate. Bagnulo et al. (2012) used the ESO FORS 1 pipeline to reduce the full content of the FORS 1 archive, among them one polarimetric observation of HD 19400 at MJD = 52852.371. While Hubrig et al. (2006a) reported for this epoch a mean longitudinal magnetic field  $\langle B_z \rangle_{\text{all}} = 151 \pm 46$  G measured using the whole spectrum and a longitudinal magnetic field  $\langle B_z \rangle_{\text{hyd}} = 217 \pm 65$  G using only the hydrogen lines, Bagnulo et al. (2012) measured  $\langle B_z \rangle_{\text{all}} = 124 \pm 85$  G, i.e. a field at a significance level of only  $1.5\sigma$ . The authors state that very small instrument flexures, negligible in most of the instrument applications, may be responsible for some spurious magnetic field detections.

Our results using high-resolution spectropolarimetry are indicative of the potential presence of a weak magnetic field in HD 19400. Applying the moment technique to Mn lines, we measure a weak negative longitudinal magnetic field  $\langle B_z \rangle = -70 \pm 23$  G at  $3\sigma$  level on the first epoch. At the same epoch the results from the SVD analysis of the observations using Mn II lines show the longitudinal magnetic field  $\langle B_z \rangle = -76 \pm 25$  G, and for the SVD analysis of Fe II lines we obtain  $\langle B_z \rangle = -91 \pm 35$  G. However, the obtained FAP values, 0.008 and 0.003, are above the value  $10^{-3}$ , and thus too high for a marginal detection according to Donati et al. (1992). We note that the presented work is based on spectra obtained only at three different nights. To get a better insight into the nature of PGa stars, it is important to carry out a more complete study based on spectropolarimetric monitoring over the rotation period.

## ACKNOWLEDGEMENTS

We thank the referee Gautier Mathys for his useful comments. Based on observations made with ESO telescopes at the La Silla Paranal Observatory under programme IDs 71.D-0308(A) and 091.D-0759(A), and data obtained from the ESO Science Archive Facility under request number MSCHOELLER51580. This work has made use of the VALD data base, operated at Uppsala University, the Institute of Astronomy RAS in Moscow, and the University of Vienna.

## REFERENCES

Alecian G., 2013, *EAS Publ. Ser.*, 63, 219  
 Alecian G., Artru M.-C., 1987, *A&A*, 186, 223  
 Alecian G., Stift M. J., Dorfi E. A., 2011, *MNRAS*, 418, 986  
 Alonso M. S., Lopez-Garcia Z., Malaroda S., Leone F., 2003, *A&A*, 402, 331  
 Artru M.-C., Freire-Ferrero R., 1988, *A&A*, 203, 111  
 Asplund M., Grevesse N., Sauval A. J., Scott P., 2009, *ARA&A*, 47, 481  
 Bagnulo S., Landstreet J. D., Fossati L., Kochukhov O., 2012, *A&A*, 538, 129

Briquet M., Korhonen H., González J. F., Hubrig S., Hackman T., 2010, *A&A*, 511, A71  
 Carroll T. A., Strassmeier K. G., Rice J. B., Künstler A., 2012, *A&A*, 548, A95  
 Castelli F., Hubrig S., 2004, *A&A*, 425, 263  
 Castelli F., Hubrig S., 2007, *A&A*, 475, 1041  
 Castelli F., Kurucz R. L., 2003, in Piskunov N., Weiss W. W., Gray D. F., eds, *Proc. IAU Symp. 210, Modelling of Stellar Atmospheres*. Astron. Soc. Pac., San Francisco, p. 20  
 Castelli F., Kurucz R. L., 2006, *A&A*, 454, 333  
 Castelli F., Kurucz R. L., 2010, *A&A*, 520, A57  
 Collado A. E., Lopez-Garcia Z., 2009, *RMxAA*, 45, 95  
 Dommanget J., Nys O., 2002, *Catalogue of the Components of Double and Multiple Stars (CCDM), Observations et Travaux*, 54, 5  
 Donati J.-F., Semel M., Rees D. E., 1992, *A&A*, 265, 669  
 Donati J.-F., Semel M., Carter B. D., Rees D. E., Collier Cameron A., 1997, *MNRAS*, 291, 658  
 Drake N. A., Hubrig S., Schöller M., Ilyin I., Castelli F., Pereira C. B., Gonzalez J. F., 2013, preprint ([arXiv:1309.5501](https://arxiv.org/abs/1309.5501))  
 Fuhr J. R., Wiese W. L., 2006, *J. Phys. Chem. Ref. Data*, 35, 1669  
 Hauck B., Mermilliod M., 1998, *A&AS*, 129, 431  
 Hubrig S., Mathys G., 1995, *Comments Astrophys.*, 18, 167  
 Hubrig S., North P., Schöller M., Mathys G., 2006a, *Astron. Nachr.*, 327, 289  
 Hubrig S., González J. F., Savanov I., Schöller M., Ageorges N., Cowley C. R., Wolff B., 2006b, *MNRAS*, 371, 1953  
 Hubrig S. et al., 2010, *MNRAS*, 408, L61  
 Hubrig S. et al., 2011, *Astron. Nachr.*, 332, 998  
 Hubrig S. et al., 2012, *A&A*, 547, A90  
 Hubrig S. et al., 2014, *MNRAS*, 440, L6  
 Ilyin I., 2012, *Astron. Nachr.*, 333, 213  
 Kling R., Schnabel R., Griesmann U., 2001, *ApJS*, 134, 173  
 Korhonen H. et al., 2013, *A&A*, 553, A27  
 Kupka F. G., Ryabchikova T. A., Piskunov N. E., Stempels H. C., Weiss W. W., 2000, *Bal. Astron.*, 9, 590  
 Kurucz R. L., 2005, *Mem. Soc. Astron. Ital. Suppl.*, 8, 14  
 Kurucz R. L., 2011, *Can. J. Phys.*, 89, 417  
 Maitzen H. M., 1984, *A&A*, 138, 493  
 Makaganiuk V. et al., 2011a, *A&A*, 525, A97  
 Makaganiuk V. et al., 2011b, *A&A*, 529, A160  
 Mathys G., 1991, *A&AS*, 89, 121  
 Mathys G., 1994, *A&AS*, 108, 547  
 Michaud G., Reeves H., Charland Y., 1974, *A&A*, 37, 31  
 Miglio A., Montalbán J., Dupret M.-A., 2007, *Commun. Asteroseismol.*, 151, 48  
 Moon T. T., 1985, *Commun. Univ. London Obs.*, 78  
 Nielsen K., Karlsson H., Wahlgren G. M., 2000, *A&A*, 363, 815  
 Piskunov N. E., Kupka F., Ryabchikova T. A., Weiss W. W., Jeffery C. S., 1995, *A&AS*, 112, 525  
 Rachkovskaya T. M., Lyubimkov L. S., Rostopchin S. I., 2006, *Astron. Rep.*, 50, 123  
 Ryabchikova T. A., Smirnov Y. M., 1994, *Astron. Rep.*, 38, 70  
 Sadakane K. et al., 2001, *PASJ*, 53, 1223  
 Scuflaire R., Théado S., Montalbán J., Miglio A., Bourge P.-O., Godart M., Thoul A., Noels A., 2008, *Ap&SS*, 316, 83  
 Sigut T. A. A., Landstreet J. D., 1990, *MNRAS*, 247, 611  
 Sigut T. A. A., Landstreet J. D., Shorlin S. L. S., 2000, *ApJ*, 530, L89  
 Sigut T. A. A., 2001, *A&A*, 377, L27  
 Snik F., Jeffers S., Keller C., Piskunov N., Kochukhov O., Valenti J., Johns-Krull C., 2008, in McLean I. S., Casali M. M., eds, *Proc. SPIE Conf. Ser. Vol. 7014, Ground-based and Airborne Instrumentation for Astronomy II*. SPIE, Bellingham, p. E22  
 Wahlgren G. M., Hubrig S., 2000, *A&A*, 362, L13  
 Wahlgren G. M., Hubrig S., 2004, *A&A*, 418, 1073  
 Yüce K., Castelli F., Hubrig S., 2011, *A&A*, 528, A37

## SUPPORTING INFORMATION

Additional Supporting Information may be found in the online version of this article:

**Table 3.** Line by line abundances of HD 19400 from the ATLAS12 model with parameters  $T_{\text{eff}} = 13\,500$  K,  $\log g = 3.9$  (<http://mnras.oxfordjournals.org/lookup/suppl/doi:10.1093/mnras/stu1122/-/DC1>).

Please note: Oxford University Press is not responsible for the content or functionality of any supporting materials supplied by the authors. Any queries (other than missing material) should be directed to the corresponding author for the paper.

This paper has been typeset from a  $\text{\TeX}/\text{\LaTeX}$  file prepared by the author.